Changes in the radiometric sensitivity of SeaWiFS determined from lunar and solar-based measurements

Robert A. Barnes, Robert E. Eplee, Jr., Frederick S. Patt, and Charles R. McClain

We report on the lunar and solar measurements used to determine the changes in the radiometric sensitivity of the Sea-viewing Wide Field-of-view Sensor (SeaWiFS). Radiometric sensitivity is defined as the output from the instrument (or from one of the instrument bands) per unit spectral radiance at the instrument's input aperture. Knowledge of the long-term repeatability of the SeaWiFS measurements is crucial to maintaining the quality of the ocean scenes derived from measurements by the instrument. For SeaWiFS bands 1–6 (412–670 nm), the change in radiometric sensitivity is less than 0.2% for the period from November 1997 through November 1998. For band 7 (765 nm), the change is approximately 1.5% and for band 8 (865 nm) approximately 5%. The rates of change of bands 7 and 8, which were linear with time for the first eight months of lunar measurements, are now slowing. The scatter in the data points about the trend lines in this analysis is less than 0.3% for all eight SeaWiFS bands. These results are based on monthly measurements of the moon. Daily solar measurements using an onboard diffuser show that the radiometric sensitivities of the SeaWiFS bands have changed smoothly during the time intervals between lunar measurements. Because SeaWiFS measurements have continued past November 1998, the results presented here are considered as a snapshot of the instrument performance as of that date.

OCIS codes: 120.0120, 030.5630, 280.0280, 300.0300, 300.6550, 300.6340.

1. Introduction

The Sea-viewing Wide Field-of-view Sensor (SeaWiFS) is a second-generation ocean color instrument. As such, its mission was designed, in large part, on the lessons learned from its predecessor, the Coastal Zone Color Scanner (CZCS). Those lessons are discussed below. In addition, SeaWiFS was developed as a data buy,[1] with the detailed design of the instrument provided by the manufacturer. However, the performance specifications included a requirement for direct lunar views to monitor instrument stability.[1] In addition, the specifications called for either an internal light source or a solar diffuser as an onboard monitor of instrument stability. The manufacturer of SeaWiFS, the Santa Barbara Research Center, chose a solar diffuser. That decision has a fundamental impact on the long-term stability monitoring program for SeaWiFS, and that impact is also discussed below.

SeaWiFS was launched on 1 August 1997 aboard the SeaStar spacecraft (now called OrbView-2). The first images of the Earth were taken on 4 September 1997, and the first lunar measurements were made on 14 November 1997. On 9 September 1997, measurements of the Sun were initiated using the onboard diffuser. Solar measurements have continued on a near-daily basis since then.

A. Coastal Zone Color Scanner Background

The Nimbus-7 CZCS was launched in October 1978. It was the first satellite sensor designed specifically for the estimation of pigment concentrations in the ocean. The mission was designed as a proof-of-concept experiment,[2] and the second generation of ocean color satellite instruments, including SeaWiFS, has been developed using the lessons learned from the CZCS experiment.[3,4] One of the most important lessons was the need for a continuous comprehensive sensor calibration evaluation activity throughout the mission. The processing of the CZCS data set was complicated by the time-dependent degradation of the scanner's radiometric sensitivity, particularly in the visible bands (little degradation could be detected in the 670- and 750-nm

R. A. Barnes, R. E. Eplee, Jr., and F. S. Patt are with General Sciences Corporation, Beltsville, Maryland 20705. C. R. McClain is with the SeaWiFS Project, Laboratory for Hydrospheric Processes, NASA Goddard Space Flight Center, Greenbelt, Maryland 20771. The e-mail address for R. A. Barnes is rbarnes@calval.gsfc.nasa.gov.

Received 24 December 1998; revised manuscript received 12 April 1999.

bands). This degradation was recognized early in the mission, but quantification of the degradation rate was difficult to assess. Although the CZCS had internal lamps, they did not illuminate the entire optical train.[5] Therefore changes in the characteristics of the optical components at the input aperture of the scanner could not be determined from measurements of the calibration lamps by the sensor. In addition, it was difficult to separate changes in the sensitivity of the instrument from changes in the outputs from those lamps.

A number of investigators applied vicarious calibration techniques to correct the CZCS calibration. Viollier[6] used a set of simultaneous *in situ* surface reflectance measurements to adjust the prelaunch calibration gain factors to yield a reasonable comparison. Gordon *et al*.[7] and Mueller[8] used field observations of the North Atlantic and North Pacific, respectively, to estimate the time dependence of the degradation by assuming that the measurements were representative for those areas. Hovis *et al*.[9] used high-altitude aircraft underflights to estimate the top-of-the-atmosphere radiances for direct comparisons with the CZCS total radiances. The most comprehensive analysis was conducted by Evans and Gordon[5] who assumed that the normalized water-leaving radiances in low-pigment open ocean waters should match the clear water values of Gordon and Clark.[10] Their analysis provided a detailed time history of the degradation of the visible bands over the entire CZCS mission. However, the method assumes that there is no systematic change in the global ocean over the 8 years of CZCS operation and does not address changes in the near-infrared bands. It is a reasonable assumption that 520 and 550 nm are constant for clear water, but may not be the case at 443 nm where small changes in pigment concentrations can produce significant fluctuations in the normalized water-leaving radiance.

With the exception of Hovis *et al*.,[9] the vicarious calibration adjustments are dependent on the particular atmospheric correction algorithm applied because the water-leaving radiances are small compared with the radiances that are due to atmospheric scattering. For such a calibration to be effective, it is necessary to separate time-dependent changes in the radiometric sensitivity of the instrument, including the near-infrared bands, from changes in the atmosphere, notably the atmospheric aerosols. As pointed out by Gordon,[11] this requires frequent and independent measurements such as images of the moon or views of the Sun through a solar diffuser. As a result, the SeaWiFS mission was designed to accommodate both of these measurements.

B. Measurement Background

SeaWiFS carries no onboard calibration standards. It has a diffuser panel that is used to measure the solar irradiance on a daily basis.[12] However, the Sun is viewed by the instrument in a manner different from measurements of the Earth, and the diffuser is not used for Earth measurements. It is an extra element used only to view the Sun. SeaWiFS carries no device, such as a ratioing radiometer,[13] to measure changes in the diffuser's reflectance. Thus, using solar measurements only, it is not possible to separate changes in the reflectance of the diffuser from changes in the radiometric sensitivity of the instrument.

For the SeaWiFS Project, there is one assumption basic to use of the solar diffuser. The change in the reflectance of the diffuser is assumed to be nearly linear for time periods up to a few months. Over longer periods, of 1 year or more, the changes can be approximately exponential with gradually decreasing changes over time. However, this exponential change can be treated as a series of linear segments. Experience with diffusers on previous satellite instruments[14,15] led to the theory that diffuser degradation on orbit is caused by the coating of the panel with photolyzed organic materials that are outgassed from the spacecraft. This accumulation of organic materials is temporally smooth and does not cause step functions in the reflectivity of the diffuser. With this assumption of short-term linear change in diffuser reflectivity, it is possible to identify sudden changes in instrument sensitivity between lunar measurements.

The SeaWiFS Project does not, as yet, use the moon as an absolute radiometric standard for calibration purposes. The moon is used solely as a diffuse reflector whose surface remains unchanged.[16] The SeaWiFS Project cannot, using its resources alone, determine the absolute reflectance of the lunar surface nor its absolute radiance. However, lunar observations by the U.S. Geologic Survey in Flagstaff, Arizona,[17,18] are being used to develop a detailed model of the moon that includes such effects as libration and phase angle on the reflectance of the lunar surface. The SeaWiFS Project maintains an active collaboration with the U.S. Geologic Survey lunar program.

SeaWiFS views the moon once a month when the moon is approximately 7° from full phase. The selection of this angle is somewhat arbitrary. Because of the inclination of the moon's orbit to the plane of the Earth's orbit around the Sun, there are months when the minimum phase angle for the full moon is greater than zero. However, for every month, the minimum phase angle is 4° or less. The 7° phase angle assures the possibility of at least one lunar measurement per month and perhaps two, one with the moon approaching full phase and one with the moon leaving. Measurements at 7° phase also maximize the illuminated surface of the moon while minimizing the opposition effect which is the rapid increase in reflected light from the lunar surface as the phase angle approaches zero. Operational considerations, such as a conflict of the lunar measurement with a midnight data downlink, will require the measurements to be moved on occasion to different phase angles. This occurred with the lunar measurement in January 1998 when the lunar phase angle for the measurement was changed to approxi-

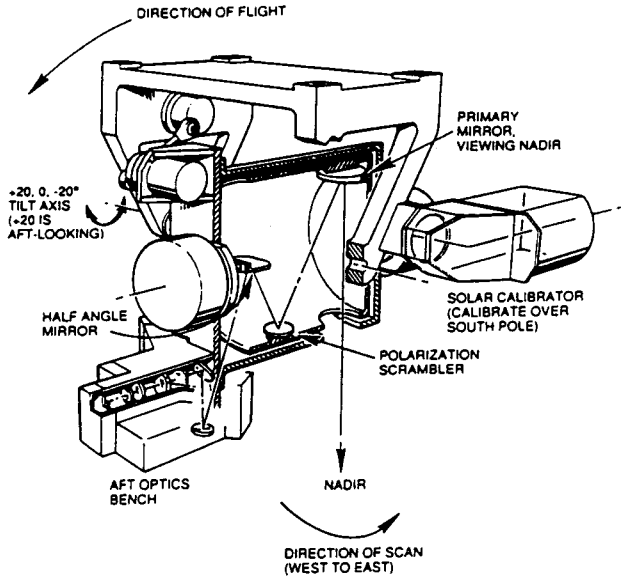

Fig. 1. SeaWiFS scanner assembly. The scanner mounts to the spacecraft using the four mounting points at the top of the figure.

mately 5.4°. There is a lunar phase change of approximately 0.8° per SeaWiFS orbit. By selecting the SeaWiFS orbit closest to 7° phase, the phase angle for each lunar measurement should be within approximately 0.5° of the desired angle.

2. Instrument Description

SeaWiFS is an eight-band filter radiometer designed to monitor Earth-exiting radiances from ocean scenes. It is the only instrument on board OrbView-2. The sensor's instantaneous field of view is 1.6 mrad by 1.6 mrad per pixel, with one scan covering 58.3° either side of nadir. SeaWiFS can be set to +20°, 0°, or −20° in the direction of flight to minimize the effects of ocean glint on the data. Each measurement is digitized to 10 bits, with a typical measurement producing approximately 600 counts with one count of noise. The results of the prelaunch characterization of SeaWiFS are summarized in Barnes *et al*.[1]

SeaWiFS consists of a scanner that contains the optics, detectors, preamplifiers, and scan mechanisms, and the electronics module that contains the signal conditioning, command and telemetry, and power supply electronics. The SeaWiFS scanner is illustrated in Fig. 1. Light first strikes the primary mirror, an off-axis parabola, and then is reflected from a second surface polarization scrambler and from the half-axis mirror before reaching the field stop. The half-angle mirror removes the rotation of the image from the scan of the telescope. The half-angle mirror uses alternating sides on successive telescope scans. After the field stop, the light is collimated by another off-axis paraboloid and directed to the aft optics assembly. Dichroic beam splitters in the aft optics divert the light into four focal plane assemblies, each containing two spectral bands delineated by narrow-band interference filters in close proximity to the detectors. Attention in the design of SeaWiFS was given to minimizing the sensitivity of the instrument to polarized light. This consideration is the principal reason for splitting the telescope into two sections, each rotating at a different speed. This design minimized the incidence angle of light on the mirrors. In addition, use of a polarization scrambler in the fore optics eliminated the need for individual scramblers to remove residual polarization at each focal plane assembly. Additional details on the design of SeaWiFS are given in Barnes and Holmes.[19]

For measurements of the Sun, SeaWiFS uses a diffuser assembly mounted to the scanner.[12] The assembly is designed so that the diffuser is illuminated by the Sun as the spacecraft passes over the South Pole. The diffuser plate is part of the diffuser housing and is painted on the inside behind a diffuser cover. The cover is also painted and acts as a second diffuser plate. The diffuser cover has a spring-loaded hinge at its bottom and is held in place by a solenoid actuator. When the one-time actuator releases the cover, it rotates out of the optical path for the diffuser. As of this writing, the diffuser cover continues to act as the instrument's diffuser plate. The plate and cover both have coatings of YB71 paint, which provides a durable flat-white coating with proven stability, as demonstrated on orbit by the Long Duration Exposure Facility. As measured by the manufacturer, the paint is spectrally flat over the measurement wavelength range of SeaWiFS.

To provide a system-level measurement of the reflectance of the diffuser, the diffuser housing was illuminated in the laboratory with a source having an angular subtense similar to the Sun. The illumination source was a 1000-W quartz halogen lamp placed approximately 305 cm from the inlet of the housing. The lamp's filament subtended an angle of approximately 1.5° at the surface of the diffuser or approximately three times the apparent diameter of the Sun as viewed from the Earth. Determining the reflectance for incident flux normal to the input aperture of the diffuser housing required two measurements. For the first measurement, the light from the lamp was measured by SeaWiFS from the diffuser. For the second, the instrument was rotated to measure the reflected light from a second diffuser. The second diffuser was made of pressed halon and was positioned to illuminate the Earth-view aperture of the instrument. The ratio of the two measurements by SeaWiFS was used to calculate the diffuser reflectance at normal incidence. For those calculations, the reflectance of the pressed halon diffuser was $0.99/\pi$. Two-dimensional reflectance tables, relative to the value at normal incidence, were determined by rotating the instrument while it viewed the halogen lamp by way of the diffuser.[12] The overall uncertainty in the laboratory characterization of the diffuser is estimated to be approximately 4%.[20] However, because we have no means of measuring the change in the reflectance of the diffuser after launch, the solar-based measurements from Sea-

0	0	0	0	0	0	0	0	0	0	0	0	0	0	0	0	0	0	0	0	0	0
0	0	0	0	0	0	0	0	0	0	0	0	0	0	0	0	0	0	0	0	0	0
0	0	0	0	0	0	0	0	0	1	0	0	0	0	0	0	0	0	0	0	0	0
0	0	0	0	0	0	1	0	1	1	0	0	0	0	0	0	0	0	0	0	0	0
0	0	0	0	0	1	3	9	31	23	3	1	0	0	0	0	0	0	0	0	0	0
0	0	0	0	1	3	6	35	121	92	11	4	2	0	0	0	0	0	0	0	0	0
0	0	0	1	0	4	19	146	303	267	88	4	4	1	0	0	0	0	0	0	0	0
0	0	0	0	1	7	39	232	399	359	155	7	4	1	1	1	0	0	0	0	0	0
0	0	0	0	3	10	96	351	457	471	312	41	5	5	0	1	0	0	0	0	0	0
0	0	0	1	5	14	140	378	439	481	380	76	3	5	2	1	2	1	0	0	0	0
0	0	0	1	6	26	225	382	406	462	446	166	0	7	3	2	1	1	0	0	0	0
0	0	0	1	6	36	264	379	406	445	466	222	1	8	3	3	2	2	1	0	0	0
0	0	0	1	7	60	317	393	412	402	471	291	7	8	4	2	2	0	0	0	0	0
0	0	0	2	9	78	343	416	419	391	463	305	11	8	4	2	2	2	1	0	0	0
0	0	2	2	10	99	365	442	429	394	421	327	24	7	4	2	3	1	0	1	0	0
0	0	1	4	10	107	375	450	443	412	399	330	28	6	4	3	1	1	1	0	0	0
0	0	0	3	11	120	388	441	479	472	392	322	29	7	4	3	2	1	1	1	0	0
0	0	1	3	12	118	399	433	509	514	408	318	27	6	4	3	1	1	1	1	0	0
0	0	1	4	11	113	428	434	541	581	454	300	21	8	4	2	2	1	1	0	0	0
0	0	0	3	11	101	438	440	553	606	480	293	16	8	5	3	3	2	2	0	0	0
0	0	1	4	10	69	413	492	590	630	530	272	7	8	5	3	2	2	1	1	0	0
0	0	0	4	10	52	380	540	634	635	550	234	4	9	4	3	2	2	0	0	0	0
0	0	0	2	9	32	275	603	708	642	539	149	3	9	3	3	1	2	1	1	0	0
0	0	0	1	6	24	209	599	735	638	478	94	5	7	3	3	1	1	0	0	0	0
0	0	0	1	5	15	96	435	668	555	295	32	6	4	2	2	2	1	1	0	0	0
0	0	0	1	3	12	58	317	540	436	180	14	6	3	1	1	2	1	0	1	0	0
0	0	0	0	2	7	21	115	274	213	49	7	4	2	0	1	1	0	0	0	0	0
0	0	0	0	1	5	12	48	129	96	19	5	2	1	1	1	0	1	0	0	0	0
0	0	0	0	0	1	5	10	17	13	3	1	0	0	0	1	0	0	0	0	0	0
0	0	0	0	0	1	1	3	5	3	0	0	0	0	0	0	0	0	0	0	0	0
0	0	0	0	0	0	0	1	1	0	0	0	0	0	0	0	0	0	0	0	0	0
0	0	0	0	0	0	0	1	0	0	0	0	0	0	0	0	0	0	0	0	0	0
0	0	0	0	0	0	0	0	0	0	0	0	0	0	0	0	0	0	0	0	0	0

Fig. 2. Lunar scene measured by SeaWiFS. The scene is 22 samples wide by 33 scan lines long. The scene is a Mercator projection with the lunar North Pole at the top. The values from band 1 are given as digital counts after the subtraction of the zero offset. For the analysis of lunar data, these counts are converted to spectral radiances using the SeaWiFS radiometric calibration algorithm.

WiFS are used solely for tracking changes in the sensor for periods between lunar measurements.

3. Lunar Measurements

SeaWiFS operates in a Sun synchronous orbit, crossing the equator from north to south at local noon. In normal operation, the spacecraft is maintained in a nadir orientation, using pitch-axis momentum wheels for attitude control with a spacecraft pitch rate of 360° per orbit. For lunar measurements, the rotation rate of the momentum wheels is increased, and the spacecraft is pitched in the opposite direction at a rate faster than normal operation. The maneuver is started past the South Pole passage and is timed such that SeaWiFS will view the moon as the spacecraft Earth track passes the sublunar point. At the end of the maneuver, approximately 28 min later, when the spacecraft again points toward the Earth, the pitch rate is returned to normal. During views of the moon, the scan direction of SeaWiFS is such that the instrument scans across the lunar surface from west to east in celestial coordinates.

Because the moon appears to be a stationary object during SeaWiFS measurements, the number of scan lines in a lunar measurement depends on the pitch rate of the instrument and the apparent size of the moon. The pitch maneuver causes SeaWiFS to oversample the moon. There are approximately 25 scan lines of the moon in the lunar image, whereas the moon has a diameter that is equivalent to approximately seven SeaWiFS samples. With a scan rate of six telescope rotations per second, the lunar image is collected in approximately 4 s.

An image of the moon is shown in Fig. 2. This image can also be considered a scene that includes the moon. Figure 2 is the scene for SeaWiFS band 1

for the first lunar measurement (November 1997). This scene gives the digital counts for each sample after the removal of the zero offset. The zero offset comes from a small, constant, internally generated voltage that ensures the digital counts in the data stream are always greater than zero. The top of the scene is celestial north, and the left side of the scene is west. Use of a 22×33 sample array for the scene allows for the inclusion of all parts of the lunar image without an excessively large number of samples of deep space.

In Fig. 2, the maximum is 735 counts. The drop off to zero counts at the top and bottom of the core of the image is approximately the same. There is no such symmetry on the left- and right-hand sides of the lunar image. This effect is due to stray light in the instrument and has been seen in laboratory testing of the instrument.[21] The moon is a good target to examine the response of SeaWiFS to bright-to-dark and dark-to-bright transitions in the scenes it measures.

The values in Fig. 2 are given as digital counts. This form of the data gives the simplest presentation of the measurements. In the SeaWiFS calibration algorithm, however, the digital counts are converted to spectral radiances for use in the analysis of the lunar measurements. There are factors in the performance of the instrument, such as the temperatures of the focal planes and side-to-side differences in the reflectance of the half-angle mirror,[22] that are part of the counts-to-spectral radiance conversion for SeaWiFS. Use of spectral radiances eliminates these instrumental factors from the lunar measurements.

For the analysis of the lunar measurements, each scene from each band for each measurement date (such as the scene in Fig. 2 for band 1 in November 1997) is represented by the disk-integrated spectral radiance. Prelaunch modeling of simulated lunar images[23] showed that disk-integrated spectral radiances produce better products than those using one, or a few, samples from the center of the image. In the lunar analysis, the summations (disk integrations) include all the samples in each 22×33 sample array. They include stray light and other instrument-based optical effects.

A. Normalizing Factors

Although the surface of the moon remains unchanged over time, the radiance from the moon does not. As a result, there are normalizing factors required for the trend analysis. These factors are based, in large part, on the spacecraft positions calculated by the SeaWiFS navigation algorithm. The navigation algorithm also provides geolocated Earth coordinates for the measurements on orbit. It also calculates the location of the instrument above the Earth's surface at the time of the lunar measurements. The SeaStar platform uses a global positioning system receiver to determine the instrument's location. The locations of the Earth and the Sun relative to the moon are derived for SeaWiFS from a calculated ephemeris as a function of the date and time of the lunar measurement.[24] With these values, five normalizing factors are calculated.

The first normalizing factor (k_1) is the Sun–moon distance. Because the Sun is an isotropic radiator, the reflected irradiance from the moon varies with the inverse square of the Sun–moon distance. The Sun–moon distance, with the moon at full phase, can be calculated as

$$D_{SM} = D_{SE} + R, \tag{1}$$

where D_{SM} is the Sun–moon distance in kilometers, D_{SE} is the Sun–Earth distance in kilometers, and R is the mean radius of the lunar orbit (3.844×10^5 km). The SeaWiFS navigation algorithm calculates the actual Earth–moon distance, which is substituted for R in Eq. (1). When the moon is farther from the Sun, it is less bright. Thus the normalizing factor k_1 gives increased values with increased Sun–Earth distance, with

$$k_1 = \left(\frac{D_{SM}}{U}\right)^2, \tag{2}$$

where k_1 is normalized to the astronomical unit U (approximately 1.496×10^8 km). The values of k_1 for the 12 lunar measurements are plotted in Fig. 3.

The second normalizing factor (k_2) is the instrument–moon distance. Because SeaWiFS is a radiometer with a small, well-defined field of view, there is no inverse square-law effect for individual samples of the lunar surface. However, this analysis uses disk-integrated spectral radiances, and the integrated image acts as an irradiance source, with

$$D_{IM} = D_{EM} - A - H, \tag{3}$$

where D_{IM} is the instrument–moon distance in kilometers, D_{EM} is the Earth–moon distance in kilometers, A is the Earth's equatorial radius (6378 km), and H is the instrument altitude above the Earth (705 km). The SeaWiFS navigation algorithm performs a more sophisticated and more exact calculation of the instrument–moon distance than that in Eq. (3). Because the moon fills fewer samples when it is farther away from the Earth, the normalizing factor is larger for larger instrument–moon distances. This factor is normalized to the mean radius of the lunar orbit, using

$$k_2 = \left(\frac{D_{IM}}{R}\right)^2. \tag{4}$$

The values of k_2 for the 12 measurements are plotted in Fig. 3.

The third normalizing factor (k_3) is the illuminated portion of the lunar surface as a function of the phase angle. This factor is a linear function of the phase of the moon, with the lunar surface fully illuminated at 0° phase, half illuminated at 90° phase, and dark at 180° phase. This function is given as

$$f_1(\theta) = a_0 + a_1\theta, \tag{5}$$

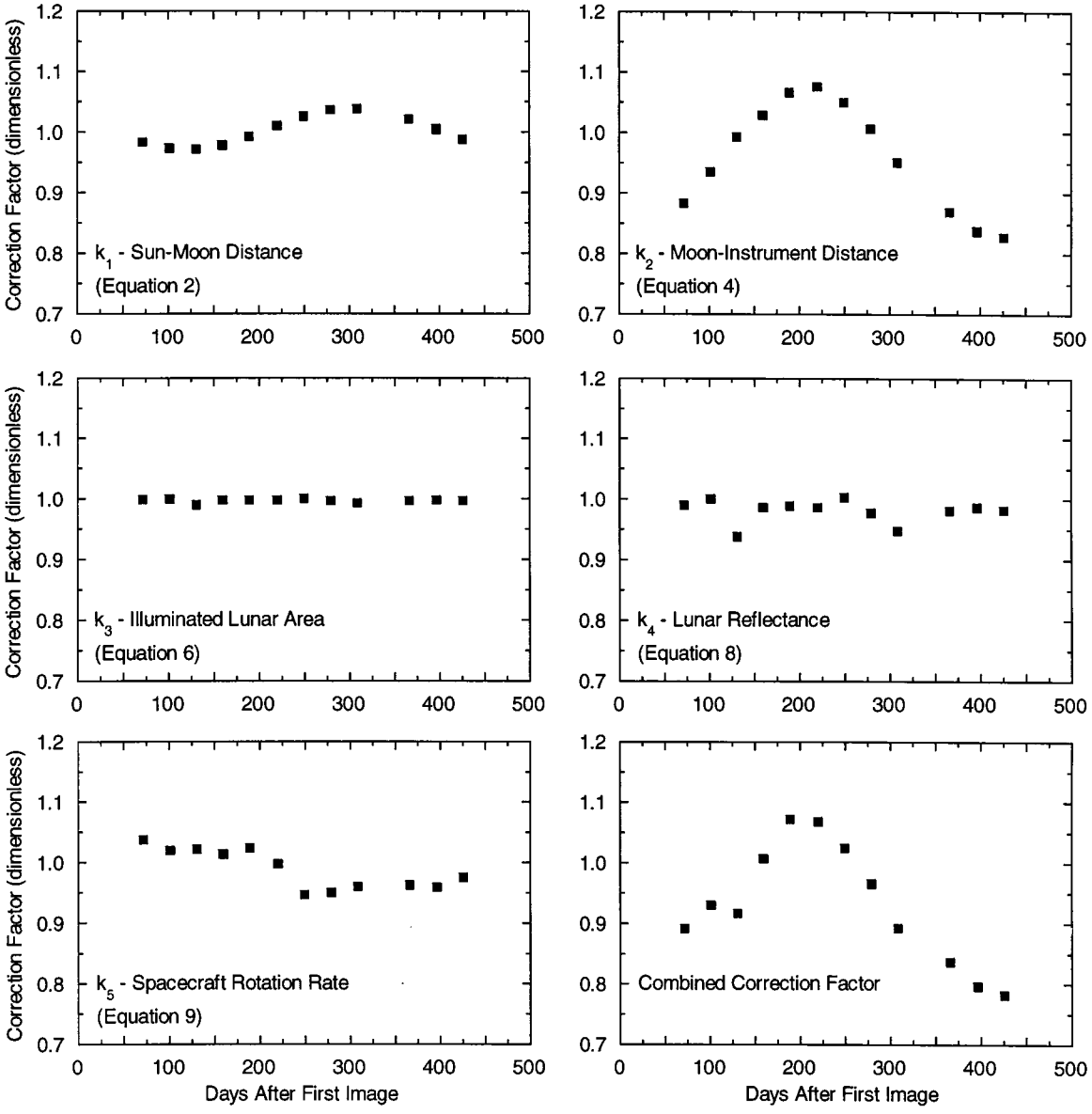

Fig. 3. Correction factors for the lunar measurements. Each individual factor is shown, plus the combined correction factor.

where $a_0 = 1$ and $a_1 = -1/180$ deg^{-1}. Factor k_3 is normalized to the fractional area of the moon illuminated at 7° from full phase, using

$$k_3 = \frac{0.9611}{a_0 + a_1\theta}. \tag{6}$$

The fourth normalizing factor (k_4) corrects for changes in the brightness of the moon with phase angle, which is a function of the change in reflectance of the moon with phase angle. The moon has a nonuniform particulate surface, creating large-scale regional variations in reflectance, such as variations between lunar mare and highlands. The non-Lambertian change in the overall reflectance of the lunar surface with phase angle can be approximated by Hapke's bidirectional reflectance equation.[25] Helfenstein and Veverka[26] used Hapke's equation, and a set of six empirically derived constants, to provide a curve of disk-integrated reflectance versus phase angle. That curve is shown in Fig. 4(a) and is given in 1° increments from 0° to 40°. The set of coefficients used by Helfenstein and Veverka[26] are based in large part on previous measurements of the lunar albedo.[27] We use a quadratic fit to provide an interpolation between the data points in Fig. 4(a). This interpolation scheme is limited to phase angles (θ's) between 3° and 11°, using the function

$$f_2(\theta) = b_0 + b_1\theta + b_2\theta^2, \tag{7}$$

where b_0 is 1.287×10^{-1}, b_1 is -6.702×10^{-3} deg^{-1}, b_2 is 2.163×10^{-4} deg^{-2}, and θ is the phase angle. The quadratic curve agrees with the values from Fig. 4(a) at the 0.1% level. The normalizing factor (k_4) is

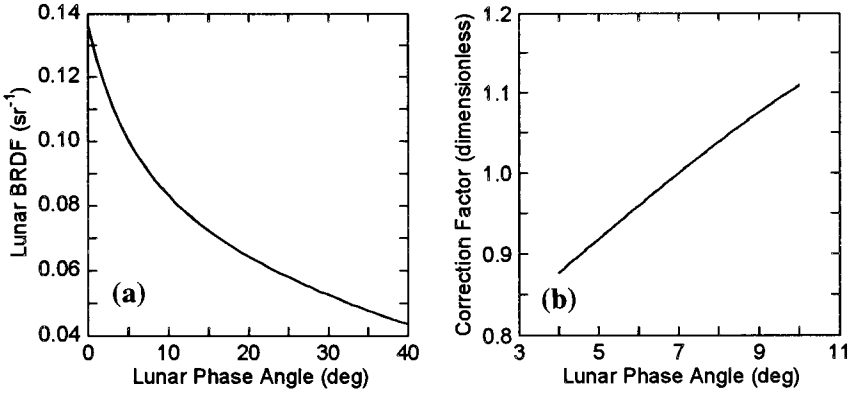

Fig. 4. Disk-integrated reflectance versus lunar phase angle: (a) disk-integrated lunar reflectance (BRDF) from 0° to 40° phase and (b) lunar reflectance normalizing factor calculated with Eq. (8). The value at 7° phase angle is unity.

calculated relative to the value at a phase angle of 7°. It is calculated as

$$k_4 = \frac{f_2(7)}{f_2(\theta)} = \frac{0.09238}{b_0 + b_1\theta + b_2\theta^2}. \tag{8}$$

The calculated values for k_4, as a function of phase angle, are shown in Fig. 4(b). There are indications that the variation in lunar reflectance with phase angle has a wavelength dependence. The normalizing factor used here is applied over a narrow range of phase angles, and it is anticipated, without complete assurance, that the effect of wavelength dependence on this normalizing factor is small. There is also evidence that the moon is brighter before full phase than after,[18] an effect of 0.5–1% in the value of k_4. However, we have not as yet developed a functional form for this dependence, and it is not applied to the values from Eq. (8).

The values of k_4 for the 12 lunar measurements are plotted in Fig. 3. For the measurements in January and July 1998 (data points 3 and 9 in Fig. 3), the phase angles for the lunar measurements were 5.4° and 5.7°, respectively.[28] For these two measurements, the values of k_4 differ from the average by 3–4%. The sensitivity of this correction factor with phase angle comes directly from the slope of the curve in Fig. 4(a). It is the reason for the restriction of the phase angles for the lunar measurements.

The fifth normalizing factor is the pitch rate of the instrument during the lunar measurement. The faster the pitch rate, the smaller the image in the direction of the pitch. Because the spacecraft does not have use of several of its positional sensors during the lunar pitch maneuver (primarily its horizon sensors), there is increased noise in its internally calculated pitch rate during measurements of the moon. As a result, we rely on the number of scan lines in the lunar image to determine the pitch rate. To do this, we find the longest vertical section in the image for each band. Using this cross section, we determine the points at which the measurement is 1% of the maximum value in the section; this is done by way of interpolation. As a result, the interval between the 1% response points is not limited to an integer number of scan lines. For each lunar measurement, the intervals for the eight bands are averaged. Because the distances between the 1% response points range from approximately 24 to 27 scan lines,[28] the results are normalized to a value of 25 scan lines, using

$$k_5 = \frac{25}{L_M \dfrac{D_{\mathrm{IM}}}{R}} = \left(\frac{25}{L_M}\right)\left(\frac{R}{D_{\mathrm{IM}}}\right), \tag{9}$$

where L_M is the interval between the 1% response points in the longest vertical section of the image. In addition, the pitch rate normalization process accounts for changes in the Earth–moon distance.

Each of the five normalizing factors used in this procedure is a fraction containing a reference constant. The overall normalizing factor for each lunar measurement (see Fig. 3) is the product of the individual factors. This multiplicative factor is applied to the summed lunar radiances for each of the eight SeaWiFS bands. It can have values as large as 1.07 and as small as 0.76. For the trend analysis, this result is further normalized to a value of unity for the first lunar measurement (November 1997).

B. Lunar Libration

The phase angle is the most important lunar surface parameter for SeaWiFS measurements of the moon. The variation of the integrated lunar radiance with phase angle is much stronger than any variation with libration angle. For libration changes, the loss of visible lunar surface from one side of the moon is balanced by the gain of visible surface from the other. The libration effect derives from the difference in reflectance of the gained surface with respect to the surface lost. This is expected to be a strong mitigating factor for the libration effect. As with lunar reflectance versus phase angle, the effect of libration is expected to be somewhat different for different wavelengths. A detailed lunar model is required to account for lunar libration. Preliminary estimates[18] show libration to be a 1–2% effect for an individual SeaWiFS lunar measurement. The complete lunar libration cycle extends for 18 years, and it is com-

posed of many subcycles of much shorter duration. For a set of lunar measurements from several months to a few years, libration is not expected to have a major effect on the slope of the time series. Rather, it is expected to increase the scatter in the data; however, the overall contribution of libration to the SeaWiFS lunar time series remains unknown to us.

C. Trends in the Lunar Measurements

The time series for the SeaWiFS measurements of the moon, covering the lunar year from November 1997 to November 1998, are shown in Fig. 5. Each of the eight time series in the figure is fitted to a straight line to give a first-order estimate of its rate of change. The figure also shows horizontal lines with values of 0.99, 1.00, and 1.01 as visual references. The data used to create Fig. 5 are listed in Table 1.

There was no lunar measurement in August 1998. At the conclusion of the July 1998 lunar maneuver, the satellite's attitude control system did not reacquire the Earth properly, causing the spacecraft to shut down and causing the loss of a few days worth of data. The correction for this problem was not fully implemented in time for the August measurement. For the last three lunar measurements in Table 1, starting in September 1998, the reacquisition of the Earth by the spacecraft was uneventful.

For SeaWiFS bands 1–6, the trend lines in Fig. 5 have upward slopes around 0.5% per year. For band 7, the trend line has a downward slope just over 1% per year, and for band 8, the annual change is downward by approximately 5%. The scatter of the data about the trend lines is approximately 0.5%, as listed in Table 2. The scatter for each band is presented in Table 2 as the standard deviation of the data points from the trend line.

There is a distinct pattern to the results in Fig. 5. For example, for each band the fifth measurement (March 1998) is highest above its trend line. This is one of five measurements taken with the moon before full phase. Because the moon is between 0.5% and 1% brighter before full phase than after,[18] this effect adds to the scatter in the measurements. The band-to-band similarities in the scatter about the trend lines are an indication that the pattern is not an instrumental effect.

The SeaWiFS geophysical algorithms use the ratios of spectral radiances from the instrument to derive its ocean data products. These band ratios use relative differences between bands, rather than relying on their absolute values. The ratio of band 7 to band 8 is used to derive the aerosol radiances in the other bands,[29] and an accurate relative calibration of these bands is essential. The derivation of surface chlorophyll concentration from ocean color measurements is simple. The water-leaving radiances from the ocean in the green portion of the spectrum do not change with chlorophyll concentration.[3] SeaWiFS band 5, at 555 nm, measures in the green. However, the water-leaving radiances in the blue bands vary inversely with the chlorophyll concentration in the surface waters because chlorophyll absorbs in the blue. The SeaWiFS geophysical algorithms use measurements from two blue bands, band 2 at 443 nm and band 3 at 490 nm, to provide the blue spectral radiances. From the blue-green color ratios, diffuse attenuation and ocean chlorophyll amounts are determined.[30,31] Use of band ratios also reduces the effects of factors common to the measurements from both bands—the effect of surface glitter, for example.

Use of band ratios can also be applied to the SeaWiFS measurements of the moon. For the lunar trend analysis, we normalized the results for each band for each month by dividing by the average value for bands 1–6 for that month. These average values are listed in the rightmost column of Table 1. The normalization to the average of bands 1–6 reduces the effects of incorrect normalizing factors common to all the bands—such as an imperfect correction for lunar phase angle. Figure 6 shows the trends in the spectral radiance ratios for the lunar measurements relative to the average for bands 1–6. As with Fig. 5, these ratios are normalized to unity for November 1997.

The trend line for band 5 is nearly flat, indicating that the normalization used for Fig. 6 is equivalent to normalizing by band 5, as is done in the SeaWiFS chlorophyll algorithm. In Fig. 6, the trend lines for bands 1 and 6 are slightly negative, the trend lines for bands 3 and 4 are slightly positive, and the trend lines for bands 2 and 5 are nearly flat. For these six bands, there is no wavelength-dependent pattern in the trends. The trends in bands 7 and 8 remain the same as those in Fig. 5.

As shown in Table 2, the scatter about the trend lines for the band ratios in Fig. 6 is significantly smaller than that for the individual band measurements in Fig. 5. We assume that this results from a reduction in the scatter from such effects as lunar libration, to the extent that the libration effect is independent of wavelength. For the geometric normalizing factors, such as the instrument–moon distance, the contribution to the scatter in the trends should be removed nearly completely. In Fig. 6, the data point for each band for March 1998 (data point 5) lies almost exactly on its trend line. Finally, the trend lines for each band in Fig. 6 have values near unity for the first lunar measurement (November 1997). This condition is not found in Fig. 5.

In a previous analysis,[28] the trends from the first nine lunar measurements from SeaWiFS were examined. In that analysis, it was concluded that there was a decrease in the radiometric sensitivity of band 6 with a rate of 0.5% annually. With the addition of three new data points (September, October, and November 1998), the slope of the band 6 trend line in Fig. 6 is very close to zero. Trend analyses can, and often do, change with the addition of new data points.

D. Nonlinear Trends

For SeaWiFS bands 7 and 8, there appears to be a reduction in their rate of change for the last three measurements, that is, for the measurements in September, October, and November of 1998. This sug-

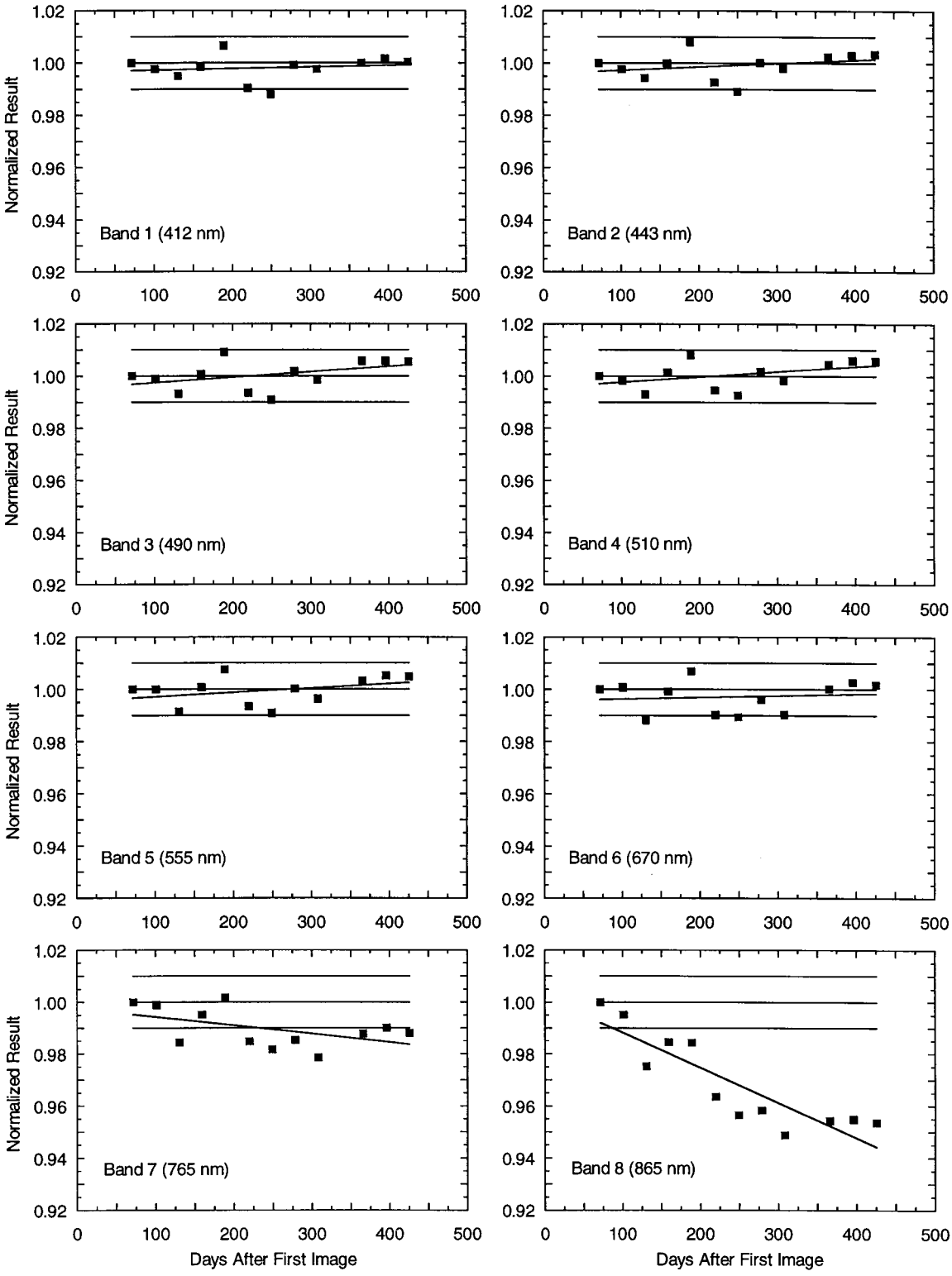

Fig. 5. Changes in radiometric sensitivities of the SeaWiFS bands from the lunar measurements. The time series are normalized to unity for the first lunar measurement in November 1997. The horizontal lines with values of 0.99, 1.00, and 1.01 are visual references.

gests that the rate of change for these bands could be approximately exponential and could approach zero change with time. These data open the possibility of alternate, nonlinear functional forms to describe changes in the instrument's radiometric sensitivity. We found that an exponential curve fit, with a small quadratic correction,

$$R_1(t) = \exp(c_0 + c_1 t + c_2 t^2), \tag{10}$$

Table 1. Data Points used to Create Fig. 5[a]

Measurement Date	Days after First Image	Band 1	Band 2	Band 3	Band 4	Band 5	Band 6	Band 7	Band 8	Average Bands 1–6
14 November 1997	71.27	1.0000	1.0000	1.0000	1.0000	1.0000	1.0000	1.0000	1.0000	1.0000
14 December 1997	100.83	0.9976	0.9978	0.9989	0.9986	1.0000	1.0008	0.9991	0.9953	0.9989
13 January 1998	130.39	0.9951	0.9943	0.9934	0.9931	0.9915	0.9886	0.9844	0.9754	0.9927
10 February 1998	159.19	0.9988	1.0001	1.0008	1.0014	1.0008	0.9993	0.9953	0.9845	1.0002
12 March 1998	188.89	1.0067	1.0081	1.0091	1.0082	1.0075	1.0068	1.0018	0.9844	1.0077
12 April 1998	219.75	0.9908	0.9928	0.9937	0.9946	0.9935	0.9905	0.9848	0.9635	0.9926
12 May 1998	249.38	0.9882	0.9892	0.9912	0.9928	0.9911	0.9893	0.9817	0.9564	0.9903
10 June 1998	278.87	0.9992	1.0002	1.0019	1.0019	1.0001	0.9963	0.9855	0.9584	0.9999
10 July 1998	308.36	0.9978	0.9982	0.9989	0.9985	0.9964	0.9905	0.9787	0.9488	0.9967
5 September 1998	366.31	0.9999	1.0026	1.0058	1.0046	1.0033	1.0002	0.9880	0.9543	1.0027
5 October 1998	395.73	1.0016	1.0032	1.0059	1.0060	1.0053	1.0026	0.9902	0.9550	1.0041
4 November 1998	425.84	1.0005	1.0035	1.0055	1.0058	1.0048	1.0017	0.9882	0.9535	1.0036

[a]The rightmost column contains the average value for the data points from bands 1–6 for each measurement date. This average is used to create Fig. 6.

fits the changes in bands 7 and 8 well. Here, $R_1(t)$ is the relative value of the trend line as a function of time t in days because the first image on orbit, and the units for the constants in the exponent, are such that the exponent is dimensionless. For each band, the values for the constants c_0, c_1, and c_2 are derived from a least-squares calculation. The trends for SeaWiFS bands 7 and 8 are shown in Fig. 7, along with the semiexponential trend lines derived with Eq. (10). The values of the trend lines are close to unity at the time of the first lunar measurement. The scatter in the data points about these trend lines is given in Table 2.

The trend lines in Fig. 7 work well over the time interval of the measurements presented here. However, SeaWiFS measurements did not stop in November 1998. As a practical matter for the production of long-term satellite-based data sets, it is important to provide a means of using the existing data to predict the radiometric sensitivity of the bands in the future. Ocean color measurements are used by the scientific community in near real time, that is, before new information on the rate of change of the instrument is available. Equation (10) suffers a major drawback as a prediction device for future instrument performance. Based on an extrapolation using the data at hand, the trend lines in Fig. 7 predict an increase in the radiometric sensitivities of bands 7 and 8 starting in early 1999. Such an improvement is contrary to our understanding of the operation of the instrument. The increase in sensitivity is allowed by the form of Eq. (10).

Table 2. Standard Deviations of the Data Points from the Trend Lines[a]

Band	Center Wavelength (nm)	Standard Deviation (Fig. 5) (%)	(Fig. 6) (%)	(Fig. 7) (%)
1	412	0.45	0.13	—
2	443	0.48	0.09	—
3	490	0.49	0.05	—
4	510	0.44	0.06	—
5	555	0.49	0.06	—
6	670	0.58	0.18	—
7	765	0.64	0.27	0.24
8	865	0.84	0.49	0.27

[a]These 1σ values are for each panel in Figs. 5, 6, and 7.

There are alternate equations that can be used to describe the change in sensitivity for bands 7 and 8. Among them is the exponential function

$$R_2(t) = 1 - d_1[1 - \exp(-d_2 t)], \tag{11}$$

where $R_2(t)$ approaches the value of $1 - d_1$ over time. Using this functional form, the prediction of an increase in radiometric sensitivity is not possible. Because of the absence of a quadratic term in the exponential of Eq. (11), the trend lines from this equation have greater stiffness than the corresponding lines based on Eq. (10). As a result, the fitted curves using Eq. (11) do not match the changes in slope of the current data for bands 7 and 8 as well as the curves in Fig. 7.

Both Eqs. (10) and (11) have another practical drawback to their use with data sets that expand over time. With the addition of each new data point to the time series, these equations recalculate the trend lines for all the previous data points. This creates an instability, as it were, for the data in the archive. Frequent changes to the data set make the data difficult, if not impossible, to use. As a result, the SeaWiFS Project uses a set of piecewise linear trend lines to track the changes in the radiometric sensitivities of bands 7 and 8. In this procedure, new segments are added to the trend line without changing previous values in the data set. Approximately once a year, there is a major reprocessing of the SeaWiFS data set. At these times it is possible to update the trend lines from the start of measurements onward.

Figure 8 shows a set of two-piece linear trend lines for SeaWiFS bands 7 and 8. The first segment for each band was calculated using a linear regression plus the first nine data points (November 1997 through July 1998). The second was calculated using the last three data points (September 1998

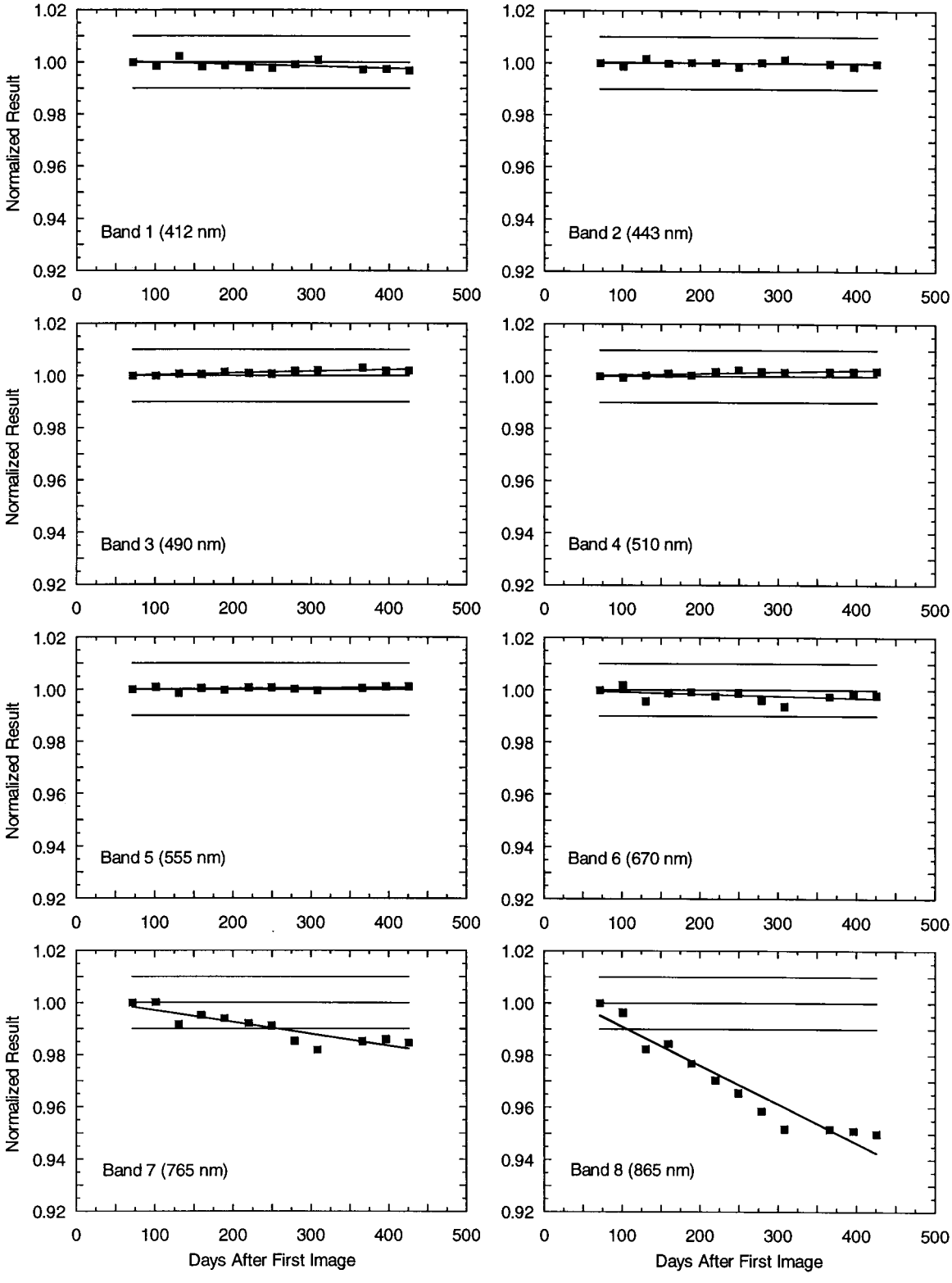

Fig. 6. Changes in the SeaWiFS bands after normalization to the average of bands 1–6. The scatter of the data points about the trend lines is substantially reduced compared with Fig. 5.

through November 1998) for band 7 and the last four data points for band 8. The incorporation of the July 1998 data point in the calculation of the second line segment for band 7 creates an upward slope for that segment. A single measurement can have a noticeable effect on the results from small data sets. Figure 8 was derived with the luxury of a lunar year's worth of data. In practice, linear segments are updated as new measurements become available. Use of several line segments has kept sharp changes in

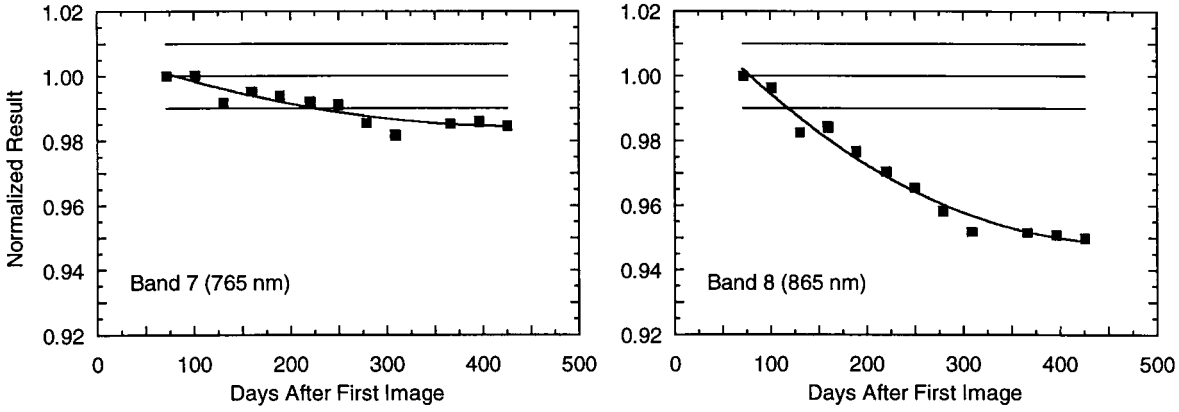

Fig. 7. Changes in SeaWiFS bands 7 and 8. The time series for these bands use the modified exponential function from Eq. (10).

slope, such as those shown in Fig. 8, out of the SeaWiFS data set. In the first half of 1999, a reprocessing of the SeaWiFS data set is planned. At that time, the current set of trend lines will be updated.

4. Solar-Based Measurements

Once in each SeaWiFS orbit when the spacecraft is over the South Pole, the rotation of the spacecraft causes the Sun to rise and set over the diffuser aperture in the direction of the spacecraft's pitch. Because of the inclination of the orbit of SeaWiFS, the incident solar irradiance also changes angle over the course of the year in the direction on the diffuser that is perpendicular to pitch. This angle is called azimuth in the nomenclature of the SeaWiFS diffuser.[12] The azimuth angles for the SeaWiFS solar measurements are shown in Fig. 9(a). They range from approximately $+5°$ to approximately $-5°$ from the normal to the plane of the input aperture of the diffuser housing. Laboratory measurements of the diffuser's bidirectional reflectance distribution function (BRDF) provide a correction for this seasonal cycle in azimuth. Because laboratory measurements were not made for all the SeaWiFS bands, the BRDF correction for band 8 is used here. It is based on Table 29 of Barnes and Eplee,[12] which gives the laboratory measurements of the diffuser cover and of the diffuser itself. For the correction used here, those measurements were fitted to a second-order polynomial curve with a value of unity at zero azimuth and a value of approximately 0.95 at 6° on each side of zero. The effect of the correction using this BRDF model is shown in Fig. 9(b). The correction increases the values of the diffuser measurements at angles where the azimuth angle is different from the normal to the input aperture of the diffuser housing, that is, from zero azimuth. The initial solar measurement with the diffuser was normalized to unity in Fig. 9(b). At day five after the first SeaWiFS image, the correction is approximately 0.6%. For band 8 (865 nm), the effect of the seasonal cycle in the azimuth angle appears to be nearly eliminated.

The solar measurements from the eight SeaWiFS bands are shown in Fig. 10. The correction for changes in the azimuth angle on the diffuser was applied to each of them. The values in Fig. 10 were selected to cover the time series for the SeaWiFS lunar measurements. They were normalized to unity on day 71. In this regard, the format of Fig. 10 duplicates that for Figs. 5 and 6. For band 1 (412 nm), there is an apparent dip in the trend line for days 100–200 after the first image. This is the time during which the solar azimuth angles on the diffuser are greater than zero. We postulate that this dip is caused by an imperfect BRDF correction. The size of the dip decreases for bands with wavelengths

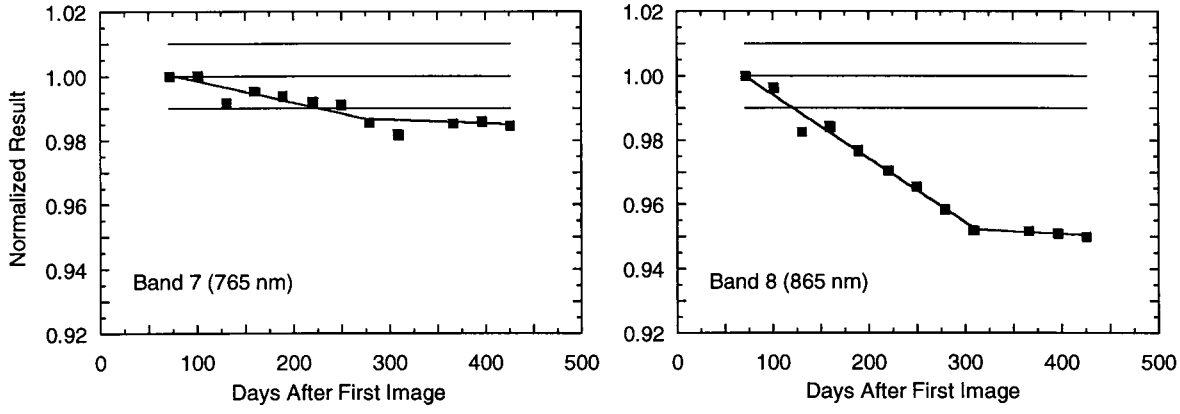

Fig. 8. Two-piece linear fits to the lunar-based trends for SeaWiFS bands 7 and 8.

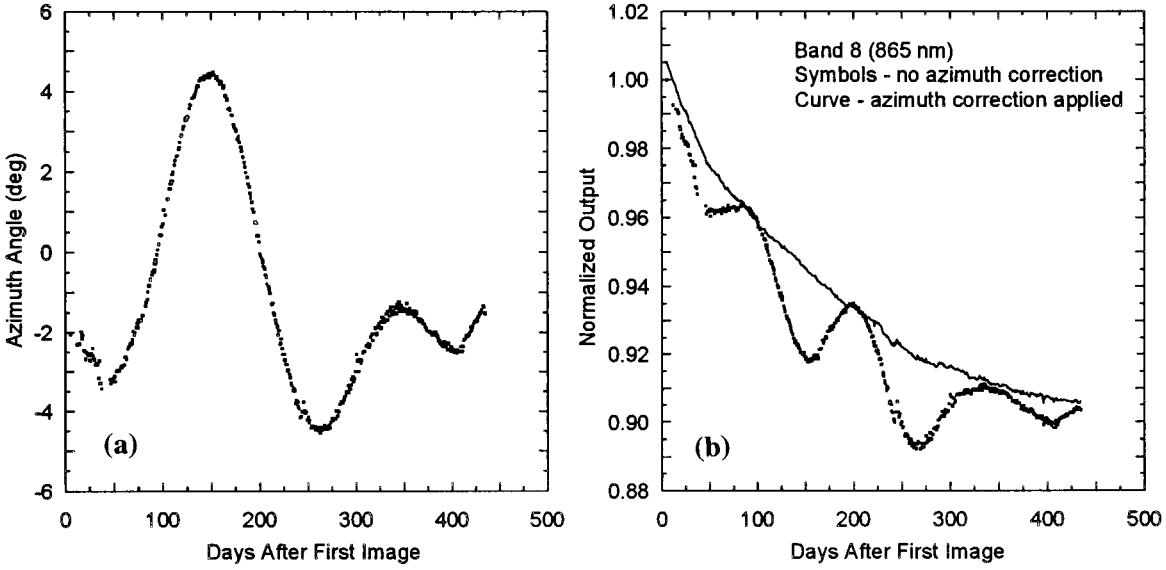

Fig. 9. Azimuth angle correction for solar diffuser measurements by SeaWiFS band 8: (a) azimuth angle for solar diffuser measurements and (b) output from band 8 before and after correction. The symbols give the values before correction and the curve gives the values after. The correction increases the values of the diffuser measurements for azimuth angles that are different from zero.

closer to that of band 8. Because the BRDF correction is based on measurements of band 8 alone, it seems likely that the imperfection in the correction increases as a function of the difference in wavelength from band 8. For band 7 (765 nm), the dip in the trend line is small but noticeable. These changes are seasonal in nature, and we assume that they will repeat from year to year. This hypothesis will be tested as SeaWiFS continues through its second year of operation. With this additional data, it may be possible to derive a correction for the repeating seasonal signature in the diffuser measurements.

There is also a long-term decrease in the diffuser measurements that is separate from the seasonal changes. For bands 1–6 there is no corresponding decrease in the lunar measurements (see Fig. 6). The changes in the diffuser measurements for bands 1–6 is consistent with the effects of the buildup of a coating on the surface of the SeaWiFS diffuser. Previous instruments, such as the solar backscatter ultraviolet radiometer onboard Nimbus-7,[15] experienced similar effects in measurements with their onboard diffusers. For these instruments, and for SeaWiFS, the long-term changes in the diffuser measurements have a wavelength dependence: The changes are greatest in the near ultraviolet and the blue, and the changes decrease with increasing wavelength. Such a trend is not seen in the diffuser measurements for SeaWiFS bands 7 and 8. For these bands, the long-term changes in the diffuser measurements appear to include the effects of the radiometric sensitivity changes shown in the lunar measurements, plus the effects of changes in the diffuser itself.

Presently our imperfect understanding of the seasonal and long-term changes in the diffuser measurements preclude their use for monitoring the radiometric sensitivity of SeaWiFS in a quantifiable manner. The diffuser measurements can be used, however, to check for sudden changes in the instrument response between lunar observations. We find no evidence of such sudden changes at the level of the short-term repeatability of the diffuser measurements, which is approximately 0.1%. This is the purpose for which the solar diffuser was incorporated into SeaWiFS. The analysis presented here also underscores the importance of a detailed characterization of the diffuser's BRDF before launch.

5. Concluding Remarks

SeaWiFS measurements of the moon show changes in the radiometric sensitivities of bands 1–6 to be small, approximately 0.2% or less for the lunar year from November 1997 to November 1998. The scatter of the data points about the trend lines is also less than 0.2% for these bands. In our analysis, each band was treated individually because each has its own interference filter and detector and amplifier system. However, in normalizing the trend data to minimize the effects of imperfections in the geometric factors, our analysis may have eliminated a change in the instrument sensitivity that is common to all the SeaWiFS bands. For example, there are optical components (including the primary telescope, polarization scrambler, and half-angle mirror) that may have changing properties effecting all the bands. There are three factors that lead us to believe that this is not the case. First, the trends for bands 1–6 in Fig. 5 are all positive; there is no sign of instrument degradation for these bands in this figure. Second, there is no sign of a wavelength dependence in the trends for bands 1–6 in Fig. 6. For changes resulting from the coating of optical surfaces, there is generally a wavelength dependence, with changes to a greater degree in the blue and changes to a lesser

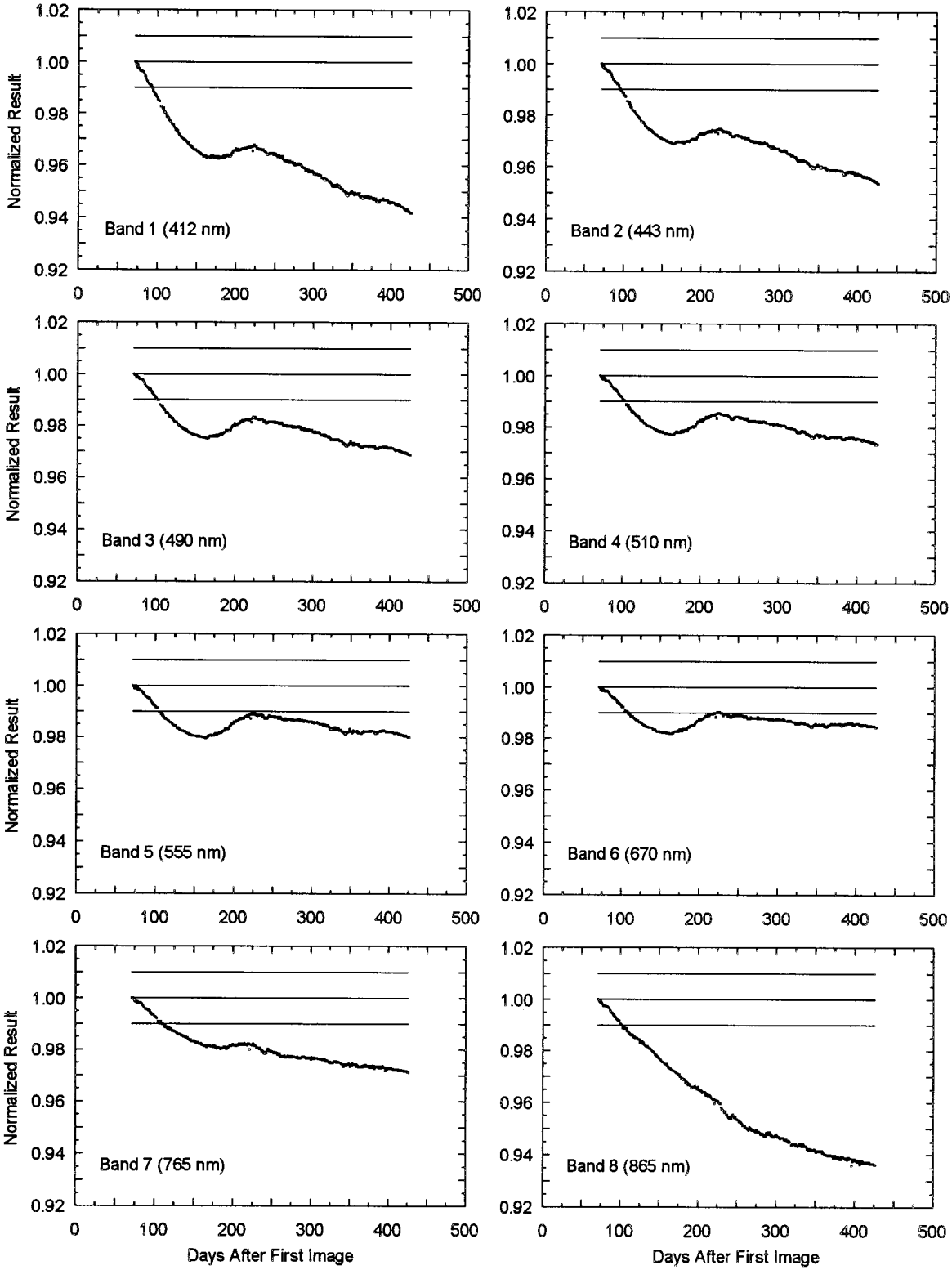

Fig. 10. Trends in the solar diffuser measurements for the SeaWiFS bands. There are 356 measurements in each panel. The format for this figure duplicates that for Figs. 5 and 6.

degree in the red. This appears be the case for the SeaWiFS diffuser for bands 1–6, as shown in Fig. 10. However, in Fig. 6 there is no sign of such a wavelength-dependent effect. And finally, there is no sign of long-term changes in the radiometric sensitivities of bands 1–6, based on comparisons with ground-truth measurements during the first year of the SeaWiFS mission.[32]

For SeaWiFS bands 7 and 8, the decreases in radiometric sensitivity over the lunar year have been

approximately 1.5% and 5%, respectively. There are signs that both rates of decrease are slowing over time. We can fit the radiometric changes in these bands to an exponentially based nonlinear function. The scatter of the data points about these trend lines for bands 7 and 8 are less than 0.3%. The exponentially based function derives from the same model that is behind self-limiting processes, such as radioactive decay, first-order chemical kinetics, and light transmission through an opaque medium (the Beer–Lambert law). However, there are practical considerations that make the use of this function, or other analytical functions, less than ideal. These include the need to predict the future radiometric sensitivities of the bands and the requirement that data points added in the future do not change the radiometric sensitivities for measurements currently in the data set.

For these reasons, the trend lines used by the SeaWiFS Project for bands 7 and 8 are a set of piecewise linear segments. Segments are added by the SeaWiFS calibration team as new lunar measurements become available. They are based on the collective judgment of the team and are used to predict future changes in bands 7 and 8. They show changes with time that are close to those in Fig. 7. A reprocessing of the SeaWiFS data set is planned for the first half of 1999. At that time there will be a reevaluation of the changes in bands 7 and 8 from the start of the SeaWiFS mission.

After consultation with the instrument manufacturer, we believe the decreases in the sensitivities of bands 7 and 8 to be caused by changes in the quantum efficiencies of the photodiodes from exposure to near-infrared radiation on orbit. This effect appears to be greater at longer wavelengths, and there is the hint in Fig. 6 of a change in band 6 (670 nm). Presumably, the degradation in the quantum efficiencies is related to the penetration of near-infrared radiation below the surface layers of the photodiodes. However, the mechanism for the changes remains unknown to us.

These changes are not caused by the circuits that amplify the outputs from the detectors. Electronic checks within SeaWiFS show the amplifiers to function normally, in the same manner as those for bands 1–6. In addition, we do not believe that the changes in sensitivity result from changes in the spectral responses of the filters. SeaWiFS carries no onboard device to check for changes in the relative spectral responses of bands 7 and 8. And a common spectral response change is possible because the two bands show structures in their spectral response curves[22] that indicate use of similar dielectric components in their construction. However, we work with the assumption that there is no shift in the spectral responses of the SeaWiFS bands. To date, the application of this assumption has proved satisfactory in the SeaWiFS atmospheric correction.

References

1. R. A. Barnes, W. L. Barnes, W. E. Esaias, and C. R. McClain, "Prelaunch acceptance report for the SeaWiFS radiometer," NASA Tech. Memo 104566 (NASA Goddard Space Flight Center, Greenbelt, Md., 1994), Vol. 22.
2. W. A. Hovis, D. K. Clark, F. Anderson, R. W. Austin, W. H. Wilson, E. T. Baker, D. Ball, H. R. Gordon, J. L. Mueller, S. Z. El-Sayed, B. Sturm, R. C. Wrigley, and C. S. Yentsch, "Nimbus-7 Coastal Zone Color Scanner: system description and initial imagery," Science **210,** 60–62 (1980).
3. S. B. Hooker, W. E. Esaias, G. C. Feldman, W. W. Gregg, and C. R. McClain, "An overview of SeaWiFS and ocean color," NASA Tech. Memo. 104566 (NASA Goddard Space Flight Center, Greenbelt, Md., 1992), Vol. 1.
4. C. R. McClain, W. E. Esaias, W. Barnes, B. Guenther, D. Endres, S. B. Hooker, B. G. Mitchell, and R. Barnes, "SeaWiFS calibration and validation plan," NASA Tech. Memo 104566 (NASA Goddard Space Flight Center, Greenbelt, Md., 1992), Vol. 3.
5. R. H. Evans and H. R. Gordon, "Coastal Zone Color Scanner system calibration: a retrospective examination," J. Geophys. Res. **99,** 7293–7307 (1994).
6. M. Viollier, "Radiance calibration of the Coastal Zone Color Scanner: a proposed readjustment," Appl. Opt. **21,** 1142–1145 (1982).
7. H. R. Gordon, J. W. Brown, O. B. Brown, R. H. Evans, and D. K. Clark, "Nimbus-7 CZCS: reduction of its radiometric sensitivity with time," Appl. Opt. **22,** 3929–3931 (1983).
8. J. Mueller, "Nimbus-7 CZCS: confirmation of its radiometric sensitivity decay," Appl. Opt. **24,** 1043–1047 (1985).
9. W. A. Hovis, J. S. Knoll, and G. R. Smith, "Aircraft measurements for calibration of an orbiting spacecraft," Appl. Opt. **24,** 407–410 (1985).
10. H. R. Gordon and D. K. Clark, "Clear water radiances for atmospheric correction of Coastal Zone Color Scanner imagery," Appl. Opt. **20,** 4175–4180 (1981).
11. H. R. Gordon, "Calibration requirements and methodology for remote sensors viewing the ocean in the visible," Remote Sens. Environ. **22,** 103–126 (1987).
12. R. A. Barnes and R. E. Eplee, Jr., "The SeaWiFS solar diffuser," in R. A. Barnes, E-n. Yeh, and R. E. Eplee, Jr., eds., *SeaWiFS Calibration Topics*, Part 1, NASA Tech. Memo. 104566 (NASA Goddard Space Flight Center, Greenbelt, Md., 1996), Vol. 39.
13. J. M. Palmer and P. N. Slater, "A ratioing radiometer for use with a solar diffuser," in *Calibration of Passive Remote Observing Optical and Microwave Instrumentation*, B. W. Guenther, ed., Proc. SPIE **1493,** 106–117 (1991).
14. J. E. Frederick, R. P. Cebula, and D. F. Heath, "Instrument characterization for detection of long-term changes in stratospheric ozone: an analysis of the SBUV/2 radiometer," J. Atmos. Oceanic Technol. **4,** 472–480 (1986).
15. J. R. Herman, R. D. Hudson, and G. N. Serafino, "An analysis of the 8 year trend in ozone depletion from alternate models of SBUV instrument degradation," J. Geophys. Res. **95,** 7403–7416 (1990).
16. H. H. Kieffer, "Photometric stability of the lunar surface," Icarus **130,** 323–327 (1997).
17. H. H. Kieffer and R. L. Wildey, "Establishing the moon as a spectral radiance standard," J. Atmos. Oceanic. Technol. **13,** 360–375 (1996).
18. H. H. Kieffer and J. M. Anderson, "Use of the moon for spacecraft calibration," in *Sensors, Systems, and Next Generation Satellite II*, H. Fujisada, ed., Proc. SPIE **3498,** 325–336 (1998).
19. R. A. Barnes and A. W. Holmes, "Overview of the SeaWiFS ocean sensor," in *Sensor Systems for the Early Earth Observing System Platforms*, W. L. Barnes, ed., Proc. SPIE **1939,** 224–232 (1993).
20. R. A. Barnes, R. E. Eplee, Jr., S. F. Biggar, K. J. Thome, E. F.

Zalewski, P. N. Slater, and A. W. Holmes, "The SeaWiFS solar radiation-based calibration and the transfer-to-orbit experiment," NASA Tech. Memo. 1999-206892 (NASA Goddard Space Flight Center, Greenbelt, Md., 1999), Vol. 5.
21. R. A. Barnes, A. W. Holmes, and W. E. Esaias, "Stray light in the SeaWiFS radiometer," NASA Tech. Memo. 104566 (NASA Goddard Space Flight Center, Greenbelt, Md., 1995), Vol. 31.
22. R. A. Barnes, A. W. Holmes, W. L. Barnes, W. E. Esaias, C. R. McClain, and T. Svitek, "SeaWiFS prelaunch radiometric calibration and spectral characterization," NASA Tech. Memo. 104566 (NASA Goddard Space Flight Center, Greenbelt, Md., 1994), Vol. 23.
23. R. H. Woodward, R. A. Barnes, C. R. McClain, W. E. Esaias, W. L. Barnes, and A. T. Mecherikunnel, "Modeling of the SeaWiFS solar and lunar observations," NASA Tech. Memo. 104566 (NASA Goddard Space Flight Center, Greenbelt, Md., 1993), Vol. 10.
24. T. C. Van Flandern and I. F. Pulkkinen, "Low-precision formulae for planetary positions," Astrophys. J. Suppl. Ser. **41,** 391–411 (1979).
25. B. Hapke, *Theory of Reflectance and Emittance Spectroscopy* (Cambridge U. Press, New York, 1993).
26. P. Helfenstein and J. Veverka, "Photometric properties of lunar terrains derived from Hapke's equations," Icarus **72,** 342–357 (1987).
27. A. P. Lane and W. M. Irvine, "Monochromatic phase curves and albedos for the lunar disk," Astron. J. **78,** 267–277 (1973).
28. R. A. Barnes, R. E. Eplee, Jr., and F. S. Patt, "SeaWiFS measurements of the moon," in *Sensors, Systems, and Next Generation Satellite II*, H. Fujisada, ed., Proc. SPIE **3498,** 311–324 (1998).
29. H. R. Gordon and M. Wang, "Retrieval of water-leaving radiances and aerosol optical thickness over the oceans with SeaWiFS: a preliminary algorithm," Appl. Opt. **33,** 443–452 (1994).
30. J. L. Mueller and C. C. Trees, "Revised SeaWiFS prelaunch algorithm for the diffuse attenuation coefficient K(490)," in *Case Studies for SeaWiFS Calibration and Validation*, E-n. Yeh, R. A. Barnes, M. Darzi, L. Kumar, E. A. Early, B. C. Johnson, J. L. Mueller, and C. C. Trees, eds., Part 4, NASA Tech. Memo. 104566 (NASA Goddard Space Flight Center, Greenbelt, Md., 1997), Vol. 41.
31. J. E. O'Reilly, S. Maritorena, B. G. Mitchell, D. A. Siegel, K. L. Carder, S. A. Garver, M. Kahru, and C. McClain, "Ocean color chlorophyll algorithms for SeaWiFS," J. Geophys. Res. **103,** 24,937–24,953 (1998).
32. C. R. McClain, M. L. Cleave, G. C. Feldman, W. W. Gregg, S. B. Hooker, and N. Kuring, "Science quality SeaWiFS data for global biospheric research," Sea Technol. **39,** 10–16 (1998).